Proceedings of ASME Turbo Expo 2011
GT2011
June 6-10, 2011, Vancouver, British Columbia, Canada

GT2011-45481

Experimental and Numerical Research of Fan Bypass Duct Flows in Japanese Environmentally Compatible Engine for Small Aircraft Project

Yoshinori Ooba
IHI Corporation
Nishitama, Tokyo, Japan

Takeshi Murooka
IHI Corporation
Nishitama,Tokyo, Japan

Takashi Yamane
Japan Aerospace Exploration Agency
Chofu, Tokyo, Japan

Osamu Nozaki
Japan Aerospace Exploration Agency
Chofu, Tokyo, Japan

Takeshi Ishiyama
ASIRI
Kanda, Tokyo, Japan

ABSTRACT

This research aims at developing fan integration technologies to improve the installation loss due to the fan/OGV/strut/pylon interaction of gas-turbine engines for small aircraft on Small Aircraft Project in Japan (the ECO Engine Project). Researches on experimental measurement using fan rig testing and numerical prediction using unsteady CFD analysis are conducted. The UPACS code which is developed by JAXA is used in order to accurately simulate the phenomena which occur in the interaction between a rotating fan and its downstream obstacles like strut/pylon in the fan duct. The accuracy of the CFD simulation is also validated by the measured data acquired in the rig testing. Through the investigations, its interaction mechanisms are clarified and the reducing technologies of such interaction for small aircraft engines are created. In the paper, the achievement of the improved aerodynamic performance by introducing the new concept of the long nose shaped fat pylon L/E are demonstrated.

INTRODUCTION

Pressure non-uniformity is particularly strong in the bypass duct due to the existence of the strut or the pylon which supports fan casing and engine core. The potential field disturbances caused by these obstacles in the form of a circumferentially varying pressure level can result in forced excitation of the fan rotor, noise generation and increased aerodynamic losses. There are various design approaches to reduce the interaction between the OGV and the strut/pylon induced field which includes an increase in the distance between the upstream components and the downstream obstacles.

Rubbert et al. was one of the first researchers who developed a concept of circumferentially varying the OGV camber angles in order to shield the fan rotor from the pressure disturbance generated by struts and pylons[1] [2]. However this type of OGV camber modification, while well known and technically very effective, is unattractive from manufacturing cost and increasing engine weight.

Kodama and Nagano performed a detailed investigation of the concept of cyclically staggering struts to control the circumferential static pressure distribution [3].

As recent aero-design approach, Tschirner, et al. investigated the influences of front geometries of thicker pylon on circumferential static pressure distribution at fan exit location using two-dimensional Computational Fluid Dynamics (CFD) simulation whose computational region included fan-bypass duct with OGV and strut and thicker pylon[4]. In the results, it was shown that static pressure distribution level can be well suppressed by combination between staggered struts and an optimized front geometry of the pylon. After these researches, Shahpar et al. applied the similar methodologies to multi-objective designing for bypass OGVs [5] [6], but the results were so restricted due to the assumption of two-dimensional CFD flowfield.

To consider three-dimensional effects of OGV/pylon interactions on the aero-design approach, Milli and Bron conducted three-dimensional CFD simulation of a fan bypass duct with OGVs and thicker pylon [7]. Their results showed that the design concept of circumferentially tailored OGV suppresses not only static pressure distribution level but also total pressure loss by controlling separated flows at OGV hub endwalls.

In the work of Unno and Kodama, the effects of a rotating fan on the OGV/strut/pylon interaction was included by simulating three-dimensional unsteady full annulus flowfield from upstream of the fan rotor to the fan nozzle exit[8]. Good agreements between simulated results and measured data of the engine test were obtained and it was indicated that this numerical approach is very effective to investigate important features of the fan/OGV/strut/pylon interaction when static pressure distribution induced by struts and pylon is not well understood.

Modern aero engines for small aircraft like regional jets are required to have more effective performance and much lower weight. In designing such engines, the axial distance between OGV and struts/pylon is required to be as short as possible in order to decrease engine length and weight. If the significantly small axial distance is inevitable and potential pressure disturbance induced by struts and pylons is not appropriately reduced, the assessment of influence of fan/OGV/strut/pylon interaction or the optimization of the strut/pylon configuration will be necessary.

Research and Technology Development in Japanese Environmentally Compatible Engine for Small Aircraft Project (ECO Engine Project) was started in 2003 and has been conducted as all Japanese collaboration program sponsored by Japanese government, Ministry of Economy, Trade and Industry (METI). The objectives of ECO Engine Project are to improve engine system integration capability and to establish advanced technologies required for the next generation small aircraft gas-turbine engines, which are environmentally friendly and economically viable[9]. For the engine design, decreased casing diameter is also essential for an engine weight reduction and a nacelle drag. A new concept of a transonic fan rotor is introduced to decrease the casing diameter without affecting the frontal area, in which the rotor hub leading edge extends toward the tip of a fan spinner. In the ultimate case where the fan rotor hub leading edge reaches to the tip of the fan spinner, then it becomes "Zero Hub to Tip Ratio Fan (ZH fan)". The ZH fan induces a flow compressed from more upstream location than other conventional fan configuration and produces a significantly high pressure ratio at hub portion, where flow enters at low radius and leaves at considerably higher radius[10] [11].

In this study, unsteady CFD simulation of three-dimensional full-annulus bypass duct with the rotating ZH fan is conducted in order to evaluate the predicted results with measured rig data and to understand the effects of the fan/OGV/strut/pylon interaction on the fan configuration of the ECO Engine Project.

NOMENCLATURE

CFD	: computational fluid dynamics
C_p	: static pressure coefficient
$C_{p(min)}$	: minimum static pressure coefficient in its circumferential distribution
L/E	: leading edge
MPI	: message passing interface
OGV	: outlet guide vane
P	: static pressure
PR	: total pressure ratio
Pt	: total pressure
T/E	: trailing edge
Tt	: total temperature
V	: velocity
W_c	: corrected mass flow rate at fan inlet
x	: axial coordinate
ZH	: zero hub-tip ratio
ρ	: density
Δ	: difference

Subscripts

design	: design point for engine
inlet	: axial location of inlet boundary condition
OGV_TE	: axial location of OGV T/E
$\overline{f}$	: mass-averaged value at same axial plane

AERODYNAMIC DESIGN AND EXPEIMENT

Figure 1 shows the cross section of designed flow path from fan rotor to OGVs with strut/pylon. A fan flow path of fan rotor and OGV was designed using an axisymmetric through flow solver. The OGV was subjected to a high inlet flow with a Mach number around one due to high pressure ratio at hub. Then design to have a backward swept leading edge geometry was introduced to reduce the influences on aerodynamic performance. A fat pylon was designed in order to install the engine to a fuselage and a thin pylon was set to locate on the opposite side of the fat pylon. The width of the fat pylon was set to contain the thrust mounting structure and tubes for the bleed air from the high pressure compressor or oil supply systems inside it.

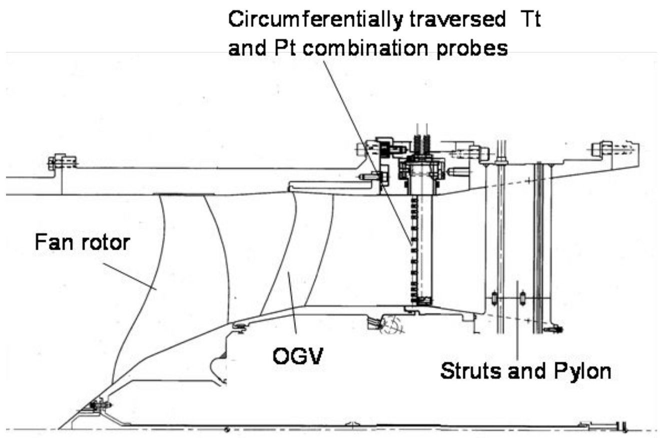

Figure 1 Cross section of fan rig test

In order to validate aerodynamic performance of the fan stage and to understand the influences of the fan/OGV/strut/pylon interaction on it, an experimental testing using a rotating fan rig was conducted by IHI. A fat pylon and a thin pylon and 6 struts were installed at downstream locations of the OGV. The fat pylon was modeled as a circular cylinder by compromising between its easy installation and constraints concerning to the rig test facility. The diameter of the fat pylon model was designed to simulate the same static pressure distribution at the downstream location of the OGV T/E as the conceptually designed engine.

The experimental data of total pressure and total temperature was measured at the fan rotor inlet and the OGV exit to evaluate the overall aerodynamic performance of the fan stage. Circumferential traverse measurement was conducted at downstream location of the OGV exit. Mass flow rate was measured using an orifice plate which was equipped at far upstream duct of the fan rotor.

Figure 2 shows the photograph of the fan rotor and figure 3 shows the photograph of the OGV/strut/pylon downstream of the fan rotor. The circumferential locations of the fat pylon and the thin pylon were set to be at 0 degree and 180 degrees, respectively. The locations of struts were 45, 90, 135, 225, 270, 315 degrees. The spanwise profiles of Pt and Tt were acquired by averaging the circumferentially traversed measurement data within one pitch spacing of the OGV passage at upstream location of 45, 135, 225 and 315 degrees positions. The static pressure level of the OGV T/E was adjusted by changing the opening of valves which were set at far downstream location of pylons and struts.

Figure 2 Photograph of front view of fan rig test

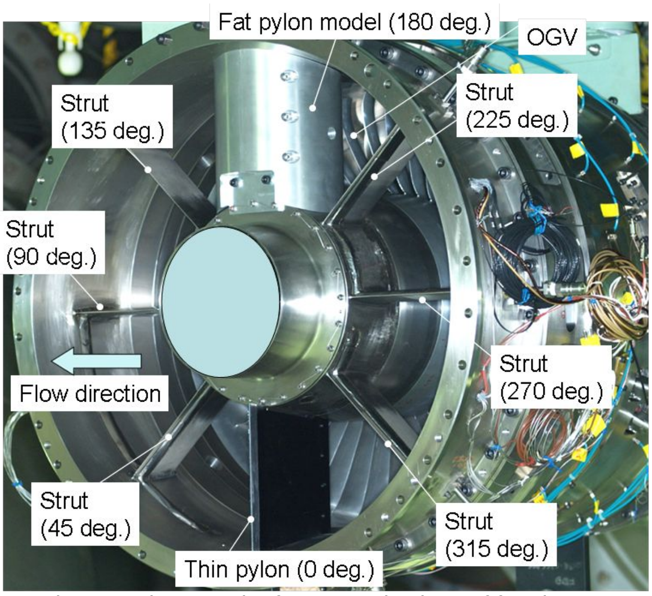

Figure 3 Photograph of struts and pylons of fan rig test (view point from downstream location of OGV)

NUMERICAL SCHEME

The CFD code used in this study is UPACS which is an unsteady three-dimensional flow solver developed by Japan Aerospace Exploration Agency (JAXA). The governing equations of the solver are the Reynolds averaged compressible Navier-Stokes equations based on a finite volume method. In this code, the convection terms are discretized by Roe's flux difference splitting method with 3^{rd}-order MUSCL, and the viscous terms are discretized by 2^{nd}-order central differences. Several turbulence model are available in this code, then turbulence viscosity is calculated using Spalart-Allmaras one-equation turbulence model base on our experiences of validation using the rig test data(12).

In the present calculation, a multi-block method with a parallel computation algorithm is introduced to simulate the full annulus computational domain from the fan rotor to far downstream location which includes OGVs, struts and pylons. The computational domain is divided into sub-domains and the calculation of each sub-domain is executed on a different processing node of JAXA Supercomputer System (JSS), which is a parallel supercomputer developed by JAXA. In the calculation, each sub-domain exchanged boundary information with neighboring sub-domains through MPI.

BOUNDARY CONDITIONS

Inlet boundary is set at upstream location of the fan spinner where total pressure, total temperature and flow angles are specified. Total pressure and total temperature of ISA condition are used for the boundary condition. Flow angles are estimated to be axial inflow condition. Outflow boundary condition is set at far downstream location of Pylons where the static pressure is specified. The static pressure level of the outflow boundary is adjusted so that calculating mass flow rate becomes close to the target operating condition. Non-slip and adiabatic wall boundary conditions are applied to fan/OGV/strut/pylon surfaces and hub/casing walls.

COMPUTATIONAL MODEL AND NUMERICAL GRID

Figure 4 shows the computational domain of the fan rig test. The passage geometry from the fan rotor to pylons is modeled. The extended axial distance upstream of the ZH fan and the far downstream region of the fat pylon model are included as the computational buffer domain. For the upstream region, the fan spinner surfaces are simulated. The flow information of the rotating fan rotor region and the OGV region is exchanged through cylindrical sub-domains at the middle axial location between the fan rotor T/E and the OGV L/E in order to effectively identify the circumferential location of neighboring sub-domains each other.

O-H type structured grid is used for each passage of cascade rows, pylons, struts. Figure 5 shows the grid arrangement at wall surfaces, the upstream region of the fan rotor and the downstream region of pylons. For cascades, pylons and struts, O-type grid surrounds the wall surfaces to keep high orthogonality on the surfaces. H-type grid is filled the spacing between the O-type grid regions. Tip clearance gaps between fan rotor blades and casing are included into the computational domain. The further upstream duct region and the fan spinner geometry are also included.

The studies of grid dependency were conducted using full annulus simulation of coarse grid[13]. In the study, not only aerodynamic performance but also detailed flowfields like connectivity of fan rotor wakes through interfaces between sub-domains were checked.

For the parallel computation, 64 CPUs of JSS is used. The computational domain is divided into 583 sub-domains, and total number of grid points is about 78,178,000. To confirm the convergence of unsteady CFD results, time history of the mass flow rate is monitored at inflow and outflow boundary locations. The needed duration to obtain the converged results in the current simulation is more than 20 fan rotor revolutions and it takes 1,125 CPU time at one operational condition.

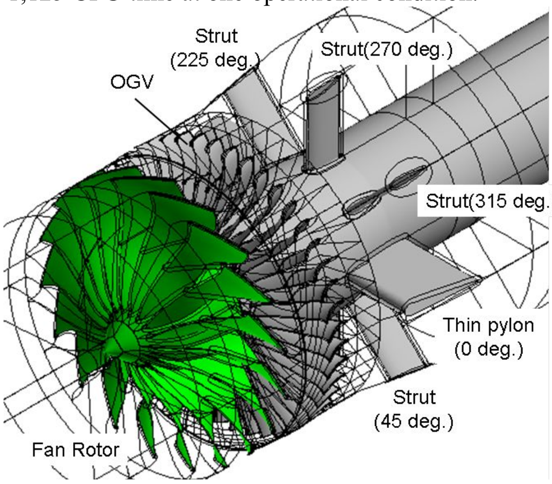

Figure 4 Computational model of fan rig test

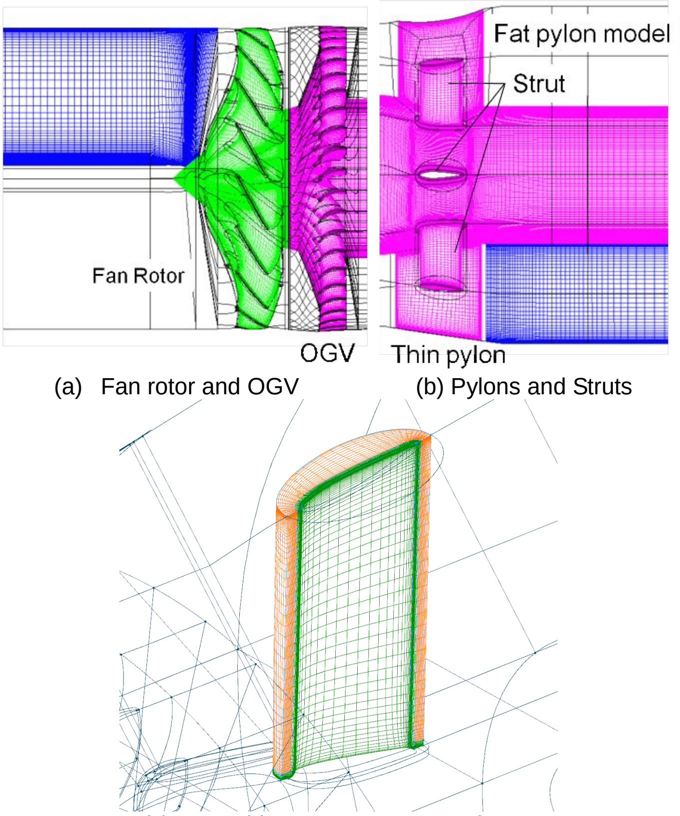

(a) Fan rotor and OGV (b) Pylons and Struts

(c) O-H grid arrangement around strut

Figure 5 Schematic of numerical grid

RESULTS AND DISCUSSION

Overall aerodynamic performance

Figure 6 shows the comparison of the fan stage performance between configurations with and without pylons. The stage performance represents measured total pressure ratio (PR) which is non-dimensionalized by PR at the design value. From the results, it is found that the fan aerodynamic performance is significantly affected due to the existence of the pylons. Especially, the PR with pylons is decreased up to 6.8% of the PR without pylons at close conditions. At the open conditions, mass flow rate of the configuration with pylons is slightly decreased than the case without pylons. It can be said that the influences of the pylons on the aerodynamic performance are more significant as decreased PR at close conditions. The solid line represents the predicted performance with the fat pylon model. The CFD predicts the similar trend of the measurement data which is slightly higher PR than the experiment.

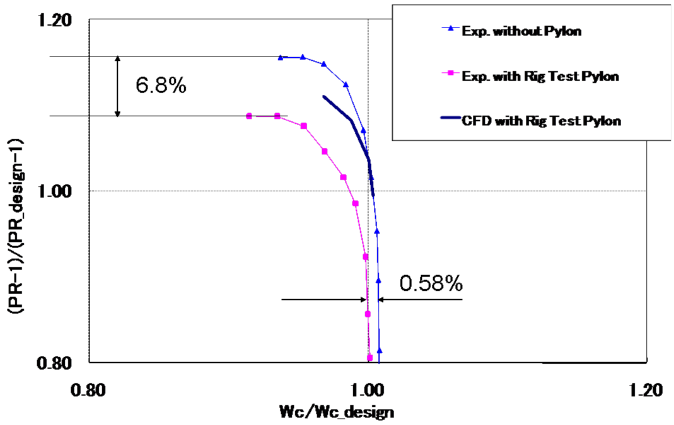

Figure 6 Comparison of aerodynamic performance between with and without pylon.

Investigation about influences due to rig pylon model

In conceptual engine designing in the Eco Engine Project, the fat pylon has a capacity to contain the required structures for engine installation to fuselage like thrust links or oil pipes inside it by adopting the blunt shaped L/E. In the fan rig test, the fat pylon model has a cylindrical geometry, then the affects concerning to its different geometry from the conceptually designed engine configuration on the flowfield is investigated using the unsteady fan duct CFD.

For the detailed study, the static pressure distributions on surfaces are compared. Figure 7 (a) shows time averaged static pressure contours on surfaces of the hub, OGV and struts of the engine pylon configuration. The static pressure is non-dimensionalized using the representative static pressure. Red region and blue region indicate higher pressure and lower pressure, respectively. The significantly higher static pressure region can be seen in front of the fat pylon L/E and the strut L/E. The high static pressure from the strut L/E decays rapidly and the affected area is restricted near its upstream location, however the high static pressure from the fat pylon L/E propagates up to OGVs. Figure 7 (b) shows static pressure contours of the rig pylon model at the same operational condition as Fig.7 (a). The higher static pressure region upstream of the strut and pylon L/E also exists and its contours are almost as same as the engine pylon configuration.

For the study of the overall characteristics, Wc-PR maps are compared each other as shown in figure 8. The green dot represents the predicted performance of the engine pylon configuration and the solid line represents the predicted one of the rig test model, respectively. The flow condition is adjusted to be the target operational condition by changing static pressure level of the outflow boundary condition at the same fan rotational speed.

There is good agreement between measured and predicted performance. From these comparisons, it can be said that the downstream shape from its maximum thickness of the fat pylon does not significantly affect the flow field just downstream of the OGV T/E and its overall aerodynamic performances.

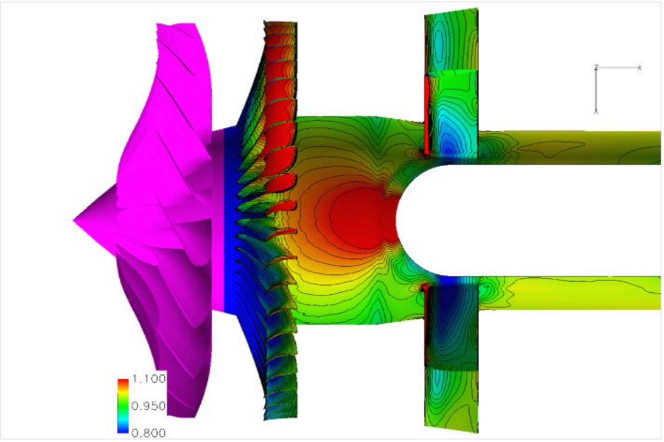

(a) Engine fat pylon configuration

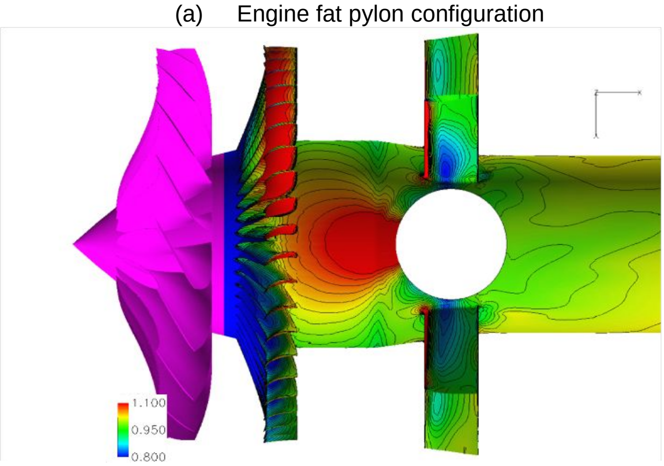

(b) Fat pylon model of fan rig test

Figure 7 Time-averaged contours of non-dimensional static pressure at near working line condition on hub casing, OGV and strut surfaces

<u>Total pressure spanwise profiles downstream of OGV</u>

Figure 9 shows the spanwise profiles of measured total pressure at four downstream locations of OGV from 45 degrees to 315 degrees. In order to understand the influence of the existence of pylons on the OGV flowfield, the measured spanwise profiles to total pressure are compared at different circumferential locations. Figure 9 (a) and (d) indicate the flow field around the thin pylon. Figure 9 (b) and (c) represent ones for the fat pylon side. From these profiles, it is found that the total pressure of the main flow around 50% spanwise location is different from the other locations. This means that there is a significant distribution in circumferential direction. From more detailed comparisons, the large deficit region of total pressure at tip portion exists from 70% spanwise location to casing surface at 45 and 315 degrees locations (see Fig. 9 (a) and (d)). The locally increased region can be also seen between 15% spanwise location and hub surface. On the other hand, the total pressure deficit at tip portion is increased at higher spanwise location than 60% span at 135 and 225 degrees location (see Fig. 9 (b) and (c)). Especially at 225 degrees location, a large total pressure deficit and reversed regions are created both at hub and tip portions. These experimental results indicate that existence of the fat pylon can strongly influence the flow field structure both of the main flow region and the secondary flow region in such small aircraft engine.

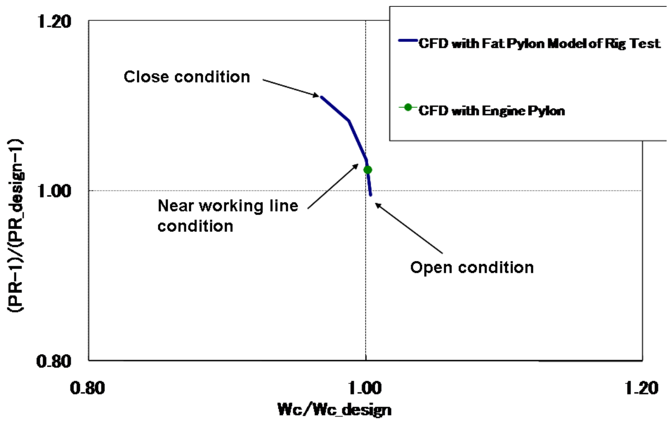

Figure 8 Comparison of aerodynamic performance between CFD results with fan rig pylon model and with engine pylon

In researches concerning to middle size aircraft engines conducted by Kodama or Unno, the influence of the potential field could be effectively sealed by OGVs and so significant influences were not achieved[(3)(8)].However, in the current investigation, such different results are observed. It is well known that the required engine mount system can not be downsized relatively to the engine size itself and the pylon of the small aircraft engine likely become larger and wider. Then it seems that the relatively wider fat pylon for small aircraft engines may enhance the influence of the potential field on the flowfield than the other class engines.

CFD results are compared with the measured data at same locations with the rig test in figure 9. The solid lines represent the time-averaged profile of predicted total pressure using CFD. From the results, it is shown that CFD can predict not only level of the total pressure but also detailed profile both of hub portion and tip portion at every measurement location. Especially, good agreement was obtained at 135 and 225 degrees location of fat pylon side. At 45 and 315 degrees locations, the discrepancy can be seen at wide spanwise range and the predicted total pressure level is slightly higher than the measured profiles. It can be a reason that the predicted aerodynamic performance by the unsteady CFD results is slightly higher than the measured data as shown in Figure 6.

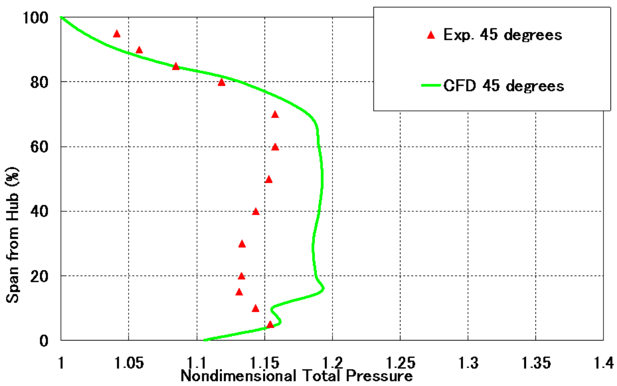

(a) 45 degrees location

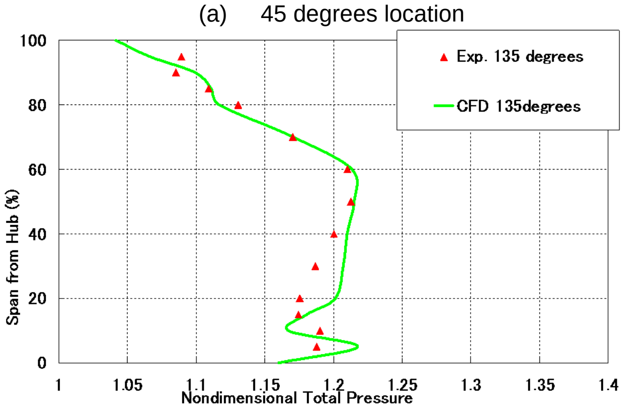

(b) 135 degrees location

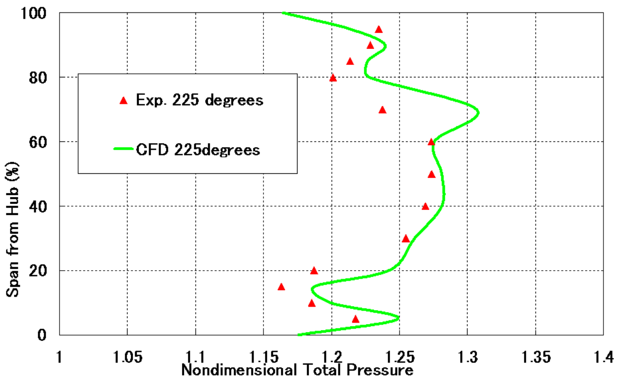

(c) 225 degrees location

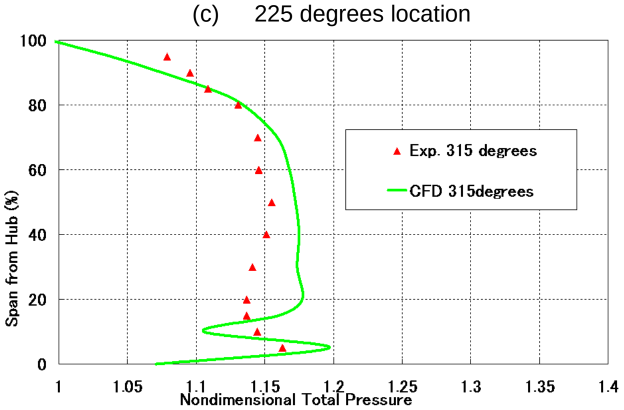

(d) 315 degrees location

Figure 9 Comparisons of total pressure spanwise profiles between CFD and measured data

Figure 10 shows time-averaged contours of non-dimensional total pressure at the circumferentially traversed measurement plane downstream of the OGV exit. The condition is the near working line as shown in figure 8. The view point is in the direction from the OGV to pylon and the rotational direction of the fan rotor is clockwise direction in these figures. The red color region represents higher total pressure and the blue region indicates lower total pressure region. As shown these figures, a significant distribution of total pressure is predicted in circumferential direction. Total pressure at the region where the fat pylon exits becomes higher than the region of the thin pylon side. Especially, the distribution has the maximum value in fan rotating direction from the fat pylon L/E.

If the inflow upstream of the OGV L/E is circumferentially uniform, such total pressure raise does not occur through stationary comportment like OGV, because external works like rotating fan are necessary to increase total pressure. This can be understood from two-dimensional CFD simulation of bypass duct OGV-pylon configurations by Tschirner et al [4]. In their simulation, circumferentially uniform inflow condition was used at upstream location of OGV L/E for different OGV-pylon configurations were investigated. In their simulation, the rotating fan was not considered. Their results showed that the fat pylon configuration and its distance from OGV T/E affected the total pressure decrease like OGV wakes or its mixing structure downstream of the OGV T/E, but total pressure of the main flow region through OGV was circumferentially similar and the total pressure raise did not occur.

Figure 11 shows the instantaneous contours of total pressure at near working line condition. The contours visualize the flowfield at midspan location of the fan duct. As seen in the figure, increased total pressure region occurs near T/E of fan passages at upstream location of the fat pylon and these increased regions go downstream through OGV passages after slightly moving according to the fan rotating direction. From these results, it can be said that this total pressure rise occurs due to the interaction between the rotating fan and OGV/strut/pylon, then the simulation in this study can predict the interaction phenomena by combining OGV/strut/pylon with the rotating fan in the computational model.

Mechanisms of the interaction phenomena can be explained as follows;

1. The circumferential distribution of static pressure is caused by the existence of the fat pylon and the obstacles in the fan duct.
2. The static pressure distribution propagates up to the OGV T/E, and the back pressure at the OGV is locally increased at upstream region of the fat pylon.
3. On the other hand, the static pressure at the OGV T/E upstream of the thin pylon is decreased to balance to the increased static pressure region.
4. The fan aerodynamic performance is strongly changed in circumferential direction due to the change of static pressure at the OGV T/E.
5. The fluid which has increased total pressure flows through OGV passages and makes total pressure increased at circumferentially wider upstream region of the fat pylon.

It also can be seen that the fluid with increased total pressure on the fat pylon side straightforwardly reaches the measured locations at 135 degrees and 225degrees. On the other hand, the total pressure on the thin pylon side can be influenced by the degree of the circumferential distribution which is determined by the mixing process of the OGV wakes or the circumferential balances of its flowfield. Then the discrepancy shown in figure 9 (a) and figure 9 (d) may occur due to the slight difference of the circumferential distribution level between the predicted results and the measured data.

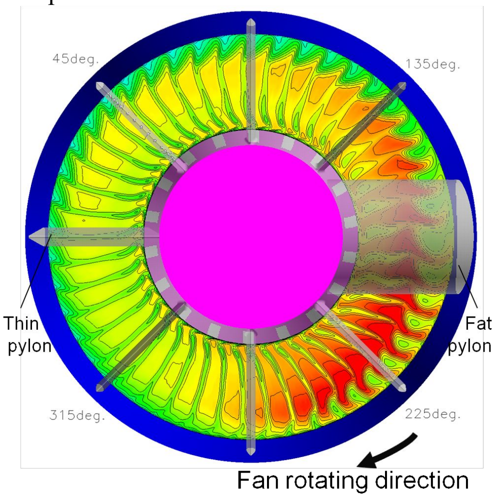

Figure 10 Time-averaged contours of total pressure at traverse measurement plane

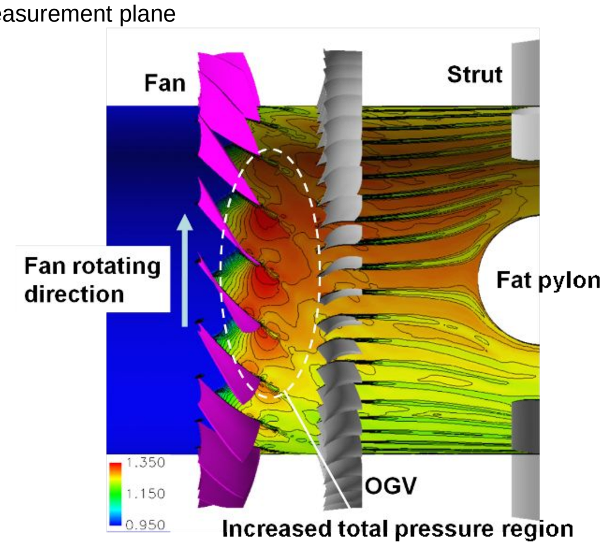

Figure 11 Instantaneous contours of non-dimensional total pressure at constant radius of fan duct midspan

To investigate the influence of the interaction on total pressure loss in the fan duct, the OGV wakes and secondary vortices are visualized at different operational conditions, as shown in figure 12. Figure 12 (a) and (b) shows the time averaged contours of total pressure of the open condition and the close condition which are seen in figure 8, respectively. OGV wakes are thin profiles stretched in spanwise direction and locally decreased region at the tip portion represents the secondary vortices. The secondary vortices near the fat pylon model L/E becomes larger than the ones near the thin pylon. This indicates that the size of secondary vortices at the tip portion is also significantly influenced by the interaction between fan and OGV/strut/pylon.

From comparison between figure 10 and figure 12, it is found that such influences on the flowfield can be changed at different operating conditions. The flowfield of the open condition is as similar as the working line condition. At the close condition, total pressure level is significantly increased and the sizes of the secondary vortices are different. The secondary vortices upstream of the fat pylon which can be seen in the working-line condition are disappeared and the size of the secondary vortices around the thin pylon is increased. Also, the secondary vortices at hub portion become larger than the open condition, so that some secondary flow from hub to tip are created. It can be seen as some helical movements of lower total pressure regions (see Fig. 12 (b)).

From these results, it can be said that the interaction between the rotating fan and obstructs like strut/pylon in bypass duct is not negligible in such small aircraft engine and the bypass duct CFD analysis which simulates OGV/strut/pylon passage by including the rotating fan can become a very useful tool to correctly understand the phenomena which occur in the flowfield of the fan and the fan bypass duct.

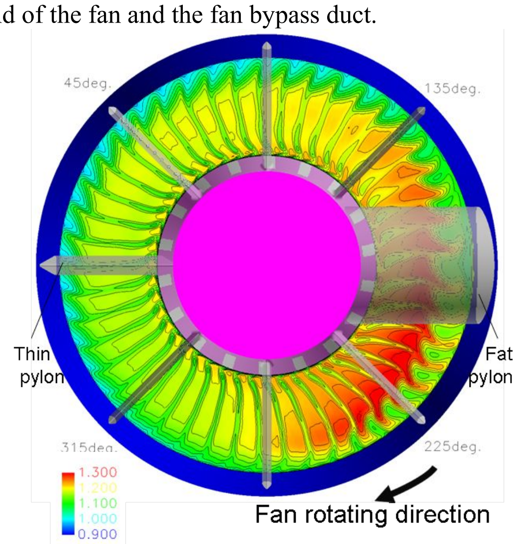

(a) Open condition

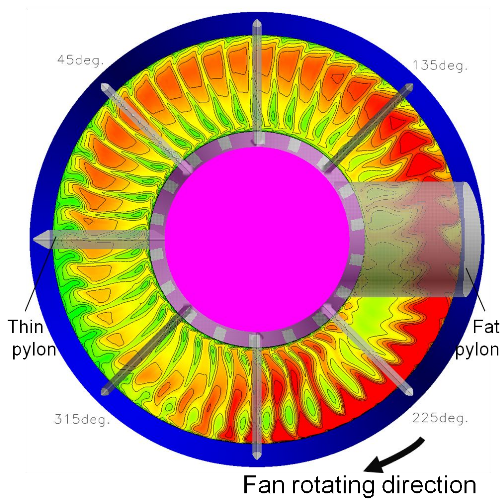

(b) Close condition

Figure 12 Comparison of time-averaged total pressure contours at different operating conditions

IMPROVEMENT OF AERODYNAMIC PERFORMANCE

Steady CFD analysis of fun duct with Strut/Pylon

Aerodynamic performance of the fan bypass duct is very important to achieve the required thrust for high bypass ratio engine configurations, because the engine thrust strongly depends on the fan nozzle pressure ratio. Improvement technology of its aerodynamic performance of the fan bypass duct is investigated by reducing the interaction between the rotating fan and the OGV/strut/pylon to decrease total pressure loss in the ECO Engine Project.

Usually, total pressure losses of the fan bypass duct are caused by the mixing phenomena of OGV/strut wakes or surface friction on the hub and surfaces and side walls of pylons.

From the unsteady CFD simulations explained in the above, it is found that the large circumferential distribution of static pressure created by the existence of the fat pylon is the governing phenomenon to enhance total pressure loss of the bypass duct. The investigation concerning to geometries of the fat pylon L/E is conducted. At first, in order to understand what geometry of the fat pylon L/E is effective to decrease the static pressure distribution and how to prevent its propagation toward the OGV T/E, the bypass duct with a fat pylon, a thin pylon and struts is simulated using steady CFD analyses. Figure 13 shows the computational domain for the steady fan duct CFD. In the steady analyses, only 180 degrees sector computational domain is calculated using symmetric boundary conditions at upstream and downstream boundaries of the fat pylon and the thin pylon which are seen as yellow surfaces in figure 13. At the inflow boundary condition, circumferentially averaged profiles of total pressure and total temperature determined by the aerodynamic design of the fan rig are used. The flow direction is set to be axial flow there. For the outflow boundary condition, the radial profile of static pressure is set and adjusted to become the same mass flow rate as the aerodynamic design. Non-slip and adiabatic wall boundary conditions are applied to strut/pylon surfaces and hub/casing walls.

In the investigation of pylon L/E geometry, the axial location of the pylon L/E and its maximum width are kept to be as same as the engine pylon configuration. The axial location of the maximum width is slightly shifted downstream by considering the required engine mount system inside it. The most interesting results are achieved for the configurations listed in table 1.

Table 1 Pylon configurations

Case	Pylon	Struts
A	Fat pylon model of fan rig test	6 struts
B	Designed Engine fat pylon	6 struts
C	Linear wedge shaped	6 struts
D	Long nose shaped	6 struts
E	Long nose shaped	2 staggered struts+ 4 w/o staggered struts

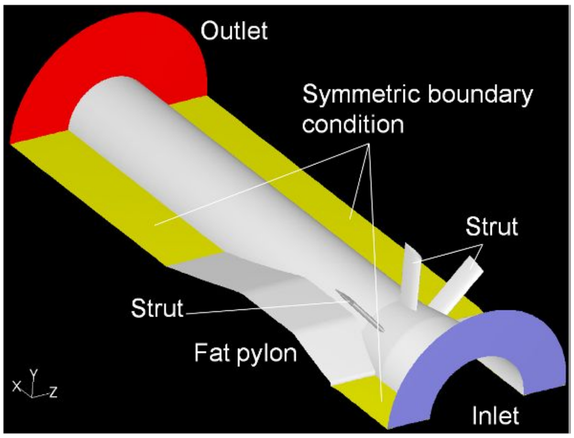

(a) Schematic of steady fan duct CFD analysis

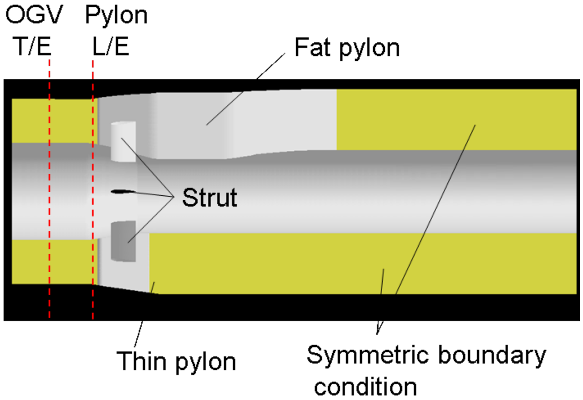

(b) Side view

Figure 13 Computational domain for steady fan duct CFD analysis

Figure 14 shows the comparison of static pressure contours at near the fat pylon L/E of 50% spanwise location from case A to case E. The red region represents high static pressure and the blue region represents low static regions. The significantly high static pressure region is predicted at upstream location of the fat pylon model similarly to the results of unsteady simulation as shown in figure 7. In the case of the linear wedge shaped configuration, the high static pressure region can be decreased because the stagnation area of the pylon L/E becomes much smaller than the fat pylon model of fan rig test. The linear wedge shaped configuration is a well-known geometry for middle size aircraft engines. The flow around the L/E is smoothly accelerated along the wedge surfaces and goes through the passage between the nearest struts and the fat pylon surface (see fig.14 (b)).

The long nose shaped configuration is a unique geometry through optimized procedure to compromise between the spacing for the engine mount system and static pressure increase at the pylon L/E. The aerodynamic concept of this configuration is as followings:

1. To locate the oblique side wall surfaces of the fat pylon as far from the OGV T/E as possible, which the static pressure is increased along.
2. To divide the high static pressure region at L/E into two regions by creating rapidly accelerating region so near the stagnation point.

As shown in figure 14 (c), the L/E geometry can successfully create the accelerated region near the stagnation point and divide the high static pressure region into the upstream stagnation location and the downstream location. By introducing the long nose shaped L/E, it becomes possible to make the high static pressure region smaller than the linear wedge shaped L/E.

In addition to the effects of the long nose shaped L/E, the two struts which locate at the adjacent location to the fat pylon (struts at 135 degrees and 225 degrees) are staggered in order to adjust the flow angle and to increase the distance between the strut T/E and the side wall surface of the fat pylon. Figure 14 (d) shows the static pressure contours of the long nose shaped L/E with staggered struts configuration. The passage between the strut and the fat pylon surface is refined, and then the high pressure region is significantly reduced.

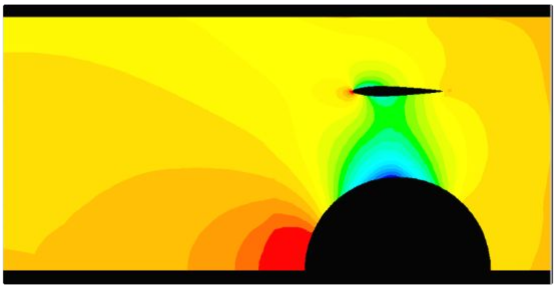

(a) Fat pylon model of fan rig test

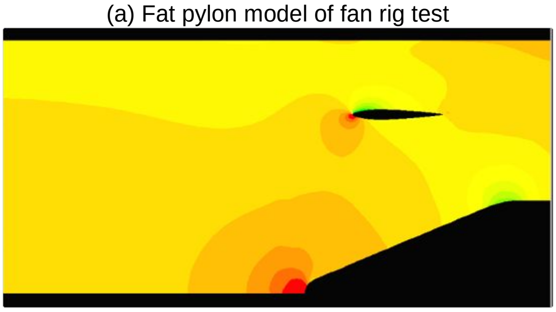

(b) Linear wedge shaped pylon L/E

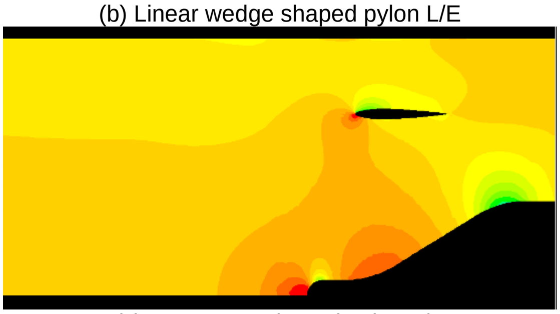

(c) Long nose shaped pylon L/E

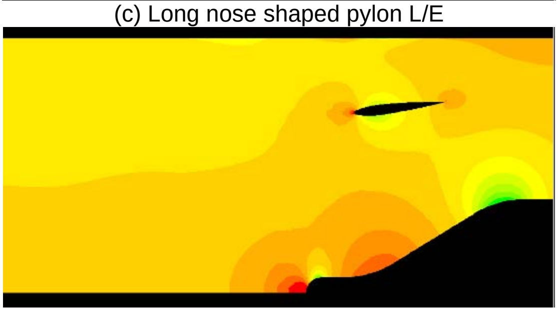

(d) Long nose shaped pylon L/E with staggered struts

Figure 14 Predicted static pressure contours at 50% spanwise location

In order to evaluate the characteristics to reduce the potential field upstream of the pylon L/E, the circumferential distributions of the static pressure are compared with each other at different axial locations of the pylon L/E and the OGV T/E as shown 15. The detailed axial locations are also indicated in figure 13 (b). The vertical axis of figure 15 (a) represents the static pressure coefficient C_p which are defined using static pressure divided by the mass-averaged dynamic pressure at the inlet boundary. In figure 15 (b), the difference of static pressure coefficient from the minimum value in its circumferential distribution ΔC_p is shown. These definitions are as following equations:

$$C_p = \frac{P}{\rho_{inlet} V_{inlet}^2} \quad \textbf{(1)}$$

$$\Delta C_p = C_p - C_p(\min) \quad \textbf{(2)}$$

At the axial location of the pylon L/E, the long nose shaped L/E can effectively reduce the peaks of static pressure coefficient at the fat pylon and the thin pylon than both of the fat pylon model and the linear wedge shaped configuration. When the static pressure propagates in the fan duct flowfield, highly variable distribution rapidly decays. Then, the circumferential distribution of static pressure coefficient varies according to the propagation process up to the axial location of the OGV T/E, because static pressure profile due to comparatively larger scales can reach to far upstream location. As shown in figure 15 (b), it is found that the long nose shaped pylon L/E with staggered struts has capability to effectively reduce the static pressure distribution in circumferential direction.

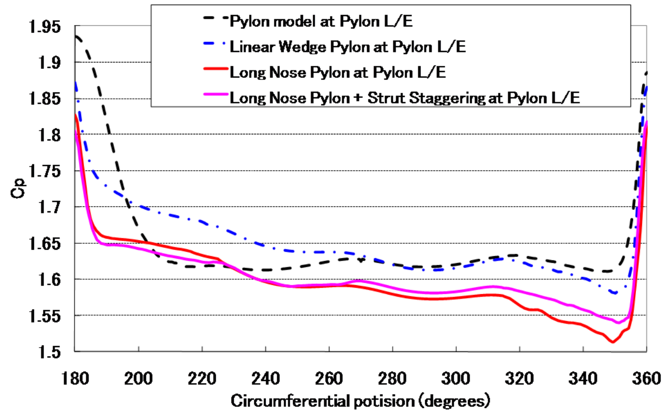

(a) *Cp* distribution at pylon L/E location

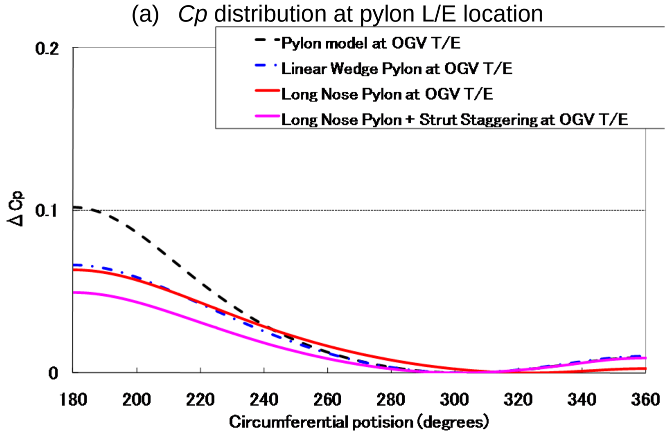

(b) *ΔCp* distribution at OGV T/E location

Figure 15 Comparison of circumferential distribution of static pressure

Evaluation of performance improvement using unsteady CFD analysis

From studies of steady fan duct CFD analyses, the effects of performance improvement by the long nose shaped fat pylon configuration are evaluated using unsteady CFD simulation which is validated using the fan rig test data. The same CFD method and same grid topology are used for the long nose shape configuration. The computational domain is divided into 591 sub-domains, and total number of grid points becomes about 81,255,000. 68 CPUs of JSS are used and it takes 768 CPU time at one operational condition. Figure 16 shows the comparison of instantaneous contours of total pressure at 50%spanwise location between case B and the refined configuration using case E. The operational condition of both configurations is near working line. As shown in this figure, the high total pressure region which occurs due to the potential field by the engine fat pylon configuration is significantly decreased in case E. The OGV wakes also smoothly flow along the passage between the fat pylon surface and adjacent struts and the mixing structure of the wakes at the location can not be seen.

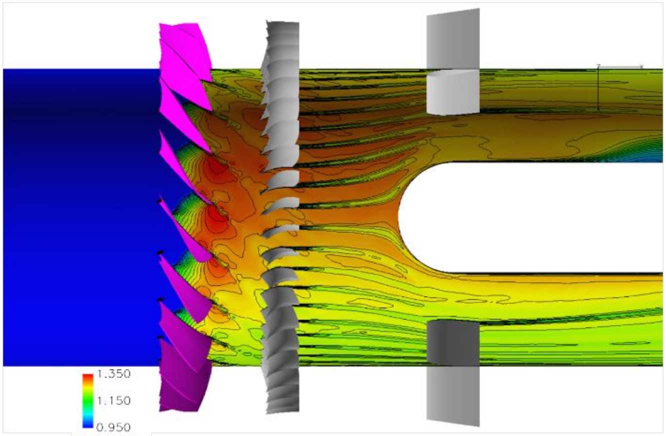

(a) Engine fat pylon configuration (case B)

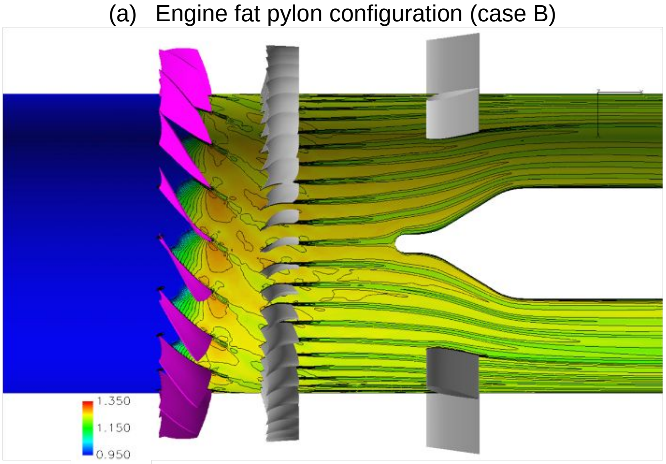

(b) Long nose shaped fat pylon configuration with staggered struts (case E)

Figure 16 Instantaneous contours of total pressure on 50% spanwise plane at near working line condition

Figure 17 shows the predicted time averaged contours of total pressure at the traverse measurement plane. In addition to reducing the circumferential distribution of the total pressure, profiles of OGV wakes become more axisymmetric than case B. The axsymmetricity of the secondary vortex regions at the tip portion are also refined, so that the low total pressure regions upstream of the fat pylon are decreased.

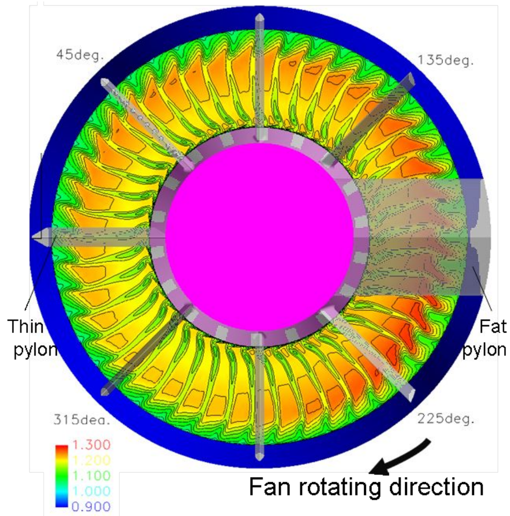

Figure 17 Time-averaged contours of total pressure of case E at traverse measurement plane

In order to evaluate the overall aerodynamic performance of the fan, the refined Wc-PR maps are compared with the predicted performance of case B as shown in figure 18. The total pressure ratio of case E is improved at all operating points. Moreover, it seems that its improvement is more effective at closed operational conditions because larger mass flow ratio and higher total pressure ratio are achieved between at the operating points between the near working line and the closed condition.

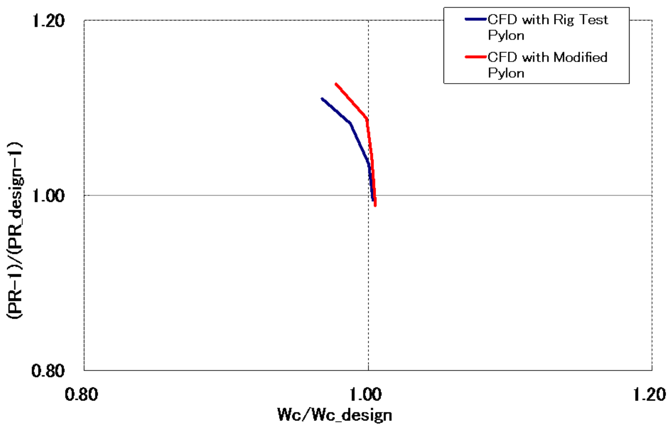

Figure 18 Comparison of aerodynamic performance by modified pylon

For the evaluation of the fan duct performance, total pressure loss coefficient is calculated using the predicted results of the unsteady fan duct CFD. The distributions along axial direction are compared between case B and case E. Here, the total pressure loss coefficient is calculated using the mass-averaged total pressure at different axial locations. Its definition is shown in equation (3). In figure 19, the horizontal axis represents the axial distance from the OGV T/E and the vertical axis represents the total pressure loss coefficient, respectively.

$$\frac{\Delta Pt}{\overline{Pt}_{OGV\_T/E}} = \frac{(\overline{Pt}_{OGV\_T/E} - \overline{Pt})}{\overline{Pt}_{OGV\_T/E}} \quad \textbf{(3)}$$

The blue solid line shows the results of case B and the red solid line represents the results of case E. The total pressure loss of case B increases from axial location of the fat pylon L/E and rapidly develops between the pylon L/E and T/E. On the other hand, the distribution of case E is slightly lower than the engine pylon configuration, however its development downstream of the pylon L/E is kept much lower than case B. So, the difference between both configurations becomes more increased the fan duct flow goes more downstream location.

From these results, the refined fan duct configuration which can effectively decrease both circumferential static pressure and the fan duct loss due to the fan/OGV/strut/pylon interaction are obtained through the current studies by combining the fan rig experimental data and the unsteady CFD analyses.

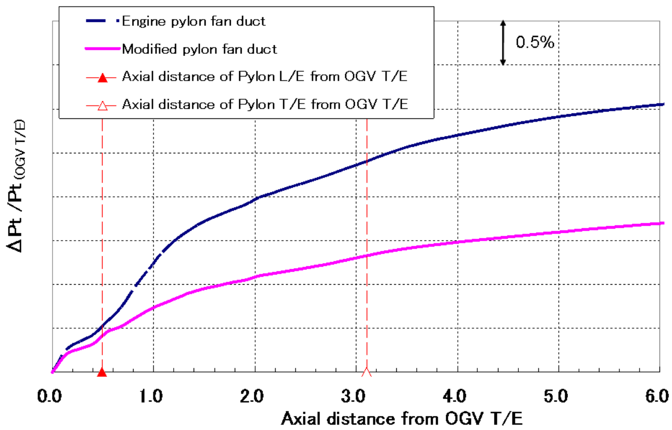

Figure 19 Comparison of total pressure loss coefficient downstream of OGV T/E

CONCLUSIONS

The experimental data of the fan/OGV/strut/pylon interaction which can occur in the small aircraft engines is acquired by conducting a fan rig test, and the influences on the aerodynamic performance of the fan and the fan duct are accurately predicted using the unsteady CFD analyses by simulating the rotating fan with OGV/strut/pylon. The work presented in this paper has demonstrated that a unique concept to decrease the interaction and the total pressure loss of the fan duct is achieved by creating a new fat pylon L/E configuration through both experimental and numerical approaches which are conducted in the ECO Engine Project.

1. The fan/OGV/strut/pylon interaction which occurs in fan and fan duct significantly may affect the flowfield of the fan duct and its aerodynamic performance especially in small aircraft engines.
2. The unsteady CFD analysis combining the rotating fan and the fan duct with strut/pylon can become a very useful tool to correctly predict the influence of the interaction on the flowfield.
3. The new concept like the long nose shaped fat pylon configuration has a capability to reasonably improve the circumferential distribution of static pressure due to the fan/OGV/strut/pylon interaction and to increase these aerodynamic performances.

ACKNOWLEDGMENTS

This study is conducted under the contract with New Energy and Industrial Technology Development Organization (NEDO) as a part of "aircraft and space industry innovation program" and "energy innovation program" of Ministry of Economy, Trade and Industry (METI).

REFERENCES

[1] Halsead D. E. et al. "Boundary Layer Development in Axial Compressors and Turbines Part 1,2,3,4", ASME-95-GT-461, 1995.

[2] Ruttert, P.E., Boctor, M.L., Cowan, S.L., and Laprete, R.D., "Concept and Design of Stators Tailored to Shield a Fan from Pressure Disturbances Arising in the Downstream Fan Duct", AIAA Paper 72-84, 1972.

[3] Kodama, H. and Nagano, S. "Potential Pressure Field by Stator/downstream Strut Interaction", Trans. ASME Journal of Turbomachinery, 111, pp.197-203, 1989.

[4] Tschirner, T., Pfitzner, M. and Merz, R., "Aerodynamic Optimization of an Aeroengine Bypass Duct OGV-Pylon Configuration", GT-2002-30493, ASME Turbo EXPO 2002, 2002.

[5] Shahpar, S., Giacche, D. and Lapworth, L., "Multi-Objective Design and Optimization of Bypass Outlet-Guide Vanes", GT2003-38700, ASME Turbo EXPO 2003, 2003.

[6] Lapworth, L. and Shahpar, S., "Design of Gas Turbine Engines Using CFD", ECCOMAS 2004, 2004.

[7] Milli, A. and Bron, O., "Fully Parametric High-Fidelity CFD Model for the Design Optimization of the Cyclic Stagger Pattern of a Set of Fan Outlet Guide Vanes", GT2009-59461, ASME Turbo Expo 2009, 2009.

[8] Unno, M. and Kodama, H. et al., "Unsteady Three-Dimensional Navier-Stokes Simulations of Fan-OGV-Strut-Pylon Interaction", ISABE 2001-1197, 2001.

[9] Funatogawa, O., Research and Technology Development in Japanese Environmentally Compatible Engine for Small Aircraft Project", ISABE-2005-1001, 2005.

[10] Goto, S., Kodama, H., "Design of Advanced Transonic Fan Rotor", AJCPP2005 D2-2, 2005.

[11] Murooka, T., Goto, S., Mizuta, I. and Kodama H., "Design and Development of and Advanced Transonic Fan Rotor", ISABE 2007-1136, 2007.

[12] Spalar, P.R. and Allmaras, S.R., "A One-Equation Turbulence Model for Aerodynamic Flows", AIAA-92-0439 1992.

[13] Ooba, Y., Murooka, T., Yamane, T., Nozaki, O. and Ishiyama, T., "Unsteady Three-dimensional Simulation Research of Fan-OGV-Strut-Pylon Interaction in Japanese ECO Engine Project", AIAA-2011-0979, 2011.